Harnessing collisional nonlinearity for enhanced harmonic generation by ultraviolet plasmonic nanoparticles

Special Collection: Plasmon-mediated Nonlinear Optics and Dynamics

Matteo Silvestri ; Matteo Venturi; Mattia Di Muzio ; Raju Adhikary ; Carino Ferrante ;
Paola Benassi ; Andrea Marini ✉

Check for updates

View Online

Export Citation

Harnessing collisional nonlinearity for enhanced harmonic generation by ultraviolet plasmonic nanoparticles

View Online   Export Citation   CrossMark

Matteo Silvestri,[1,a] (iD) Matteo Venturi,[1] Mattia Di Muzio,[1] (iD) Raju Adhikary,[1] (iD) Carino Ferrante,[2] (iD)
Paola Benassi,[1,2] (iD) and Andrea Marini[1,2,b] (iD)

AFFILIATIONS

[1] Department of Physical and Chemical Sciences, University of L'Aquila, Via Vetoio, 67100 L'Aquila, Italy
[2] CNR-SPIN, c/o Dip.to di Scienze Fisiche e Chimiche, Via Vetoio, Coppito (L'Aquila) 67100, Italy

Note: This paper is part of the JCP Special Topic on Plasmon-mediated Nonlinear Optics and Dynamics.
[a] matteo.silvestri@univaq.it
[b] Author to whom correspondence should be addressed: andrea.marini@univaq.it

ABSTRACT

We investigate the contribution of inelastic electron collisions to nonlinear (NL) dynamics in ultraviolet plasmonic nanoparticles, exploring their potential for harmonic generation. Employing the Landau weak coupling formalism to model radiation-driven electron dynamics in sodium and aluminum, we account for both electron–electron and electron–phonon scattering processes by a set of hydrodynamic equations, which we solve perturbatively to obtain third-order NL susceptibilities. Furthermore, we model high harmonic generation enhanced by localized surface plasmons in nanospheres composed of such poor metals, demonstrating their efficient operation for extreme ultraviolet generation. Our investigation reveals that plasmonic nanospheres composed of sodium and aluminum produce a large field intensity enhancement of $\simeq 10^3$–10^5, boosting the harmonic generation process. Our findings indicate that poor metals hold great promise for advanced extreme ultraviolet nano-sources with potential applications in nano-spectroscopy.

I. INTRODUCTION

Harnessing nonlinear (NL) effects in nanoscaled photonic systems is crucial for several applications encompassing low-power frequency conversion,[1] NL switching,[2] and soliton formation.[3] Indeed, because NL effects in isotropic systems depend over the field intensity, they can get enhanced by the subwavelength localization properties of surface plasmons (SPs),[4–6] collective electrostatic excitations of electrons in nanostructures composed of metals or semi-metals. Surface-induced nonlinearity enhancement by surface plasmon polariton (SPP)[7,8] and localized plasmon (LP)[9,10] resonances has been adopted for diverse NL plasmonic applications based on noble metals, mainly operating in the visible spectral domain. However, the large absorption of noble metals in the visible range poses a stringent limitation on the NL functionalities of plasmonic devices. In turn, absorption mitigation, for example, by surface roughness reduction[11] or SPP amplification by externally pumped active media,[12–15] plays an important role for advancing plasmon-enhanced NL functionalities. Moreover, the adoption of infrared (IR) plasmonic materials, for example, graphene,[16,17] oxides, and nitrides,[18–20] produces absorption mitigation thanks to electron density reduction.

IR plasmonic media also offer appealing epsilon-near-zero (ENZ) features[21] that enhance nonlinearity[22] and can be exploited in a number of photonic applications,[23] for example, NL tunneling control,[24] enhanced harmonic generation,[25,26] and frozen solitary doughnut formation.[27] Furthermore, ENZ media enable high harmonic generation (HHG)[28] that can be exploited to develop ultraviolet (UV) radiation sources,[29,30] holding great potential for micromachining and special marking.[31] However, because HHG in solids does not ensue from multiphoton tunneling ionization like in atoms,[32] extreme ultraviolet (XUV) generation by IR ENZ media is

18 December 2024 14:12:57

not efficient due to the high harmonic order required to reach photon energies >10 eV in the XUV spectral regime. For this reason, the adoption of UV plasmonic materials such as poor metals[21] is promising for XUV generation, manipulation, and guidance.[33]

Here, we investigate the potential of plasmonic nanospheres (NSs) based on poor metals, particularly sodium (Na) and aluminum (Al), for plasmon-enhanced harmonic generation. Because Na and Al do not undergo interband dynamics in the visible–UV spectral range, they are particularly promising plasmonic media with mitigated absorption and a purely intraband Drude-like electromagnetic (EM) response. In turn, the NL properties of such materials ensue mainly from electron plasma dynamics damped by inelastic collisions with the ionic lattice background, which we account for by the Landau weak coupling formalism and by a previously reported generalized hydrodynamic model (GHM) accounting for electron–electron and electron–ion grazing collisions non-perturbatively.[34] Collision-driven third-harmonic generation (THG) NL susceptibilities of Al and Na are obtained by previously reported analytical expressions obtained through the perturbative solution of the GHM.[35] By considering Na/Al-based NSs illuminated by EM pump pulses with ≃ps time duration, we solve the scattering problem in the electrostatic regime, obtaining analytical expressions for the radiated THG power in the undepleted pump approximation. We find that such NSs produce a large field intensity enhancement of $\simeq 10^5$, boosting the harmonic generation process. Finally, by numerically solving the GHM in the local response regime through a fourth-order Runge Kutta algorithm, we evaluate the ultrafast heating dynamics of electrons over the ≃ps timescale, finding that Na/Al-based NSs produce efficient HHG due to the fast temporal oscillations of the nonlinearly-saturated instantaneous absorbed power density. Our results shed light on the opportunities offered by poor metals for advanced NL plasmonic applications.

II. COLLISION-DRIVEN NONLINEARITY

We model collision-driven nonlinearity of Na and Al by a previously reported GHM,[34,35] whose derivation and working principles are briefly summarized in this section. Owing to the nonresonant electronic response of bulk Na and Al in the visible–UV spectral range, their EM response is dominated by plasma dynamics that can be evaluated within the classical kinetic theory framework. Here, the conduction electrons are treated as a dilute plasma while the lattice ions with mass M are regarded as a homogeneous thermal bath of positive charge at equilibrium temperature T_0 = 300 K with distribution function $f_0(\mathbf{r}, \mathbf{w}) = n_0 (M/2\pi k_b T_0)^{3/2} \exp(-Mw^2/2k_b T_0)$, where $\mathbf{w}$ is the microscopic velocity, $\mathbf{r}$ is the position vector, n_0 is the lattice ion density, and k_b is the Boltzmann constant. The temporal evolution of the electron distribution function $f(\mathbf{r}, \mathbf{w}, t)$ is governed by the Boltzmann equation,

$$\partial_t f + \mathbf{w} \cdot \nabla_\mathbf{r} f + \frac{1}{m} \mathbf{F}_\mathbf{w}(\mathbf{r}, t) \cdot \nabla_\mathbf{w} f = (\partial_t f)_{\text{coll}}, \qquad (1)$$

where $\mathbf{F}_\mathbf{w}(\mathbf{r}, t) = -e\mathbf{E}(\mathbf{r}, t) - e\mathbf{w} \times \mathbf{B}(\mathbf{r}, t)$ is the external EM force exerted by the electric $\mathbf{E}(\mathbf{r}, t)$ and magnetic $\mathbf{B}(\mathbf{r}, t)$ pump fields, $-e$ and m are the electron charge and effective mass, respectively, and $(\partial_t f)_{\text{coll}} = (\partial_t f)_{\text{coll}}^{\text{el–el}} + (\partial_t f)_{\text{coll}}^{\text{el–ph}}$ is the total collision rate resulting from electron–electron (el–el) $[(\partial_t f)_{\text{coll}}^{\text{el–el}}]$ and

electron–phonon (el–ph) $[(\partial_t f)_{\text{coll}}^{\text{el–ph}}]$ collisions. The Landau weak coupling formalism enables the evaluation of $(\partial_t f)_{\text{coll}}$, where frontal el–el and el–ion (producing phonons) collisions are disregarded and only grazing collisions are retained.[34,35] This leads to the expression of $(\partial_t f)_{\text{coll}}$ in differential form through the introduction of NL Rosenbluth potentials.[34,35] In turn, Eq. (1) is solved by the Landau method of moments (truncated at the second moment) and the non-perturbative calculation of $(\partial_t f)_{\text{coll}}$.[34,35] The local temporal evolution of the moments $\mathbf{v}(\mathbf{r}, t)$ (first-order, mean velocity) and $T_e(\mathbf{r}, t)$ (second-order, temperature) is governed by

$$\partial_t \mathbf{v}(\mathbf{r}, t) = \frac{1}{m} \mathbf{F}_{\text{eff}}(\mathbf{r}, t) - \gamma \mathcal{F}_\gamma(\mathbf{v}, T_e) \mathbf{v}(\mathbf{r}, t), \qquad (2a)$$

$$\partial_t T_e(\mathbf{r}, t) = Q(\mathbf{v}, T_e), \qquad (2b)$$

where $\mathbf{F}_{\text{eff}} = -e\mathbf{E} - e\mathbf{v} \times \mathbf{B}$ is the external effective force, γ is the linear damping rate, and $\mathcal{F}_\gamma$ and Q are the NL damping and heating rates,[34,35] respectively, explicitly given by

$$\mathcal{F}_\gamma(\mathbf{v}, T_e) = \frac{3v_{T0}^3}{2v^2 v_T} \left[\mathcal{G}(v/v_T) - e^{-\frac{v^2}{v_T^2}} \right], \qquad (3a)$$

$$Q(\mathbf{v}, T_e) = \gamma_{\text{th}} \frac{Mv_{T0}^3}{2k_b v_T} \left[\mathcal{G}(v/v_T) - \frac{T_e v_{T0}^2}{T_0 v_T^2} e^{-\frac{v^2}{v_T^2}} \right]. \qquad (3b)$$

In the expressions above $\mathcal{G}(\mathbf{v}, T_e) = \sqrt{\pi} v_T \text{erf}(v/v_T)/2v$, $\gamma_{\text{th}} = 2m\gamma/(m + M)$ is the linear thermal relaxation rate coefficient, and $v_T(T_e) = \sqrt{2k_b(T_0/M + T_e/m)}$ and $v_{T0} = v_T(T_0)$ are the electron thermal velocities in out-of-equilibrium and equilibrium conditions, respectively. Such GHM accounts for ultrafast heating and its effect on the induced current density $\mathbf{J}(\mathbf{r}, t) = -en_0\mathbf{v}(\mathbf{r}, t)$, and has been previously adopted to model out-of-equilibrium electron dynamics in silver[34] and THG in Na-based thin films.[35] Here, we adopt the GHM to derive (i) novel analytical expressions for THG polarizabilities of Na/Al-based nanospheres (see Sec. III), and (ii) to model plasmon-enhanced HHG non-perturbatively (see Sec. IV). In our calculations, we consider a Na/Al-based NS with diameter D immersed in vacuum and illuminated by an ultrafast pulse with time duration $\tau \simeq 0.1$–1 ps (intensity full-width at half-maximum), peak intensity I_0, and carrier vacuum wavelength λ_0 (angular frequency $\omega_0 = 2\pi c/\lambda_0$, where c is the speed of light in vacuum), see Fig. 1(a). In turn, the impinging pump electric field is given by $\mathbf{E}_0(\mathbf{r}, t) = \text{Re}[\mathbf{a}_0(t - z/c)e^{ik_0 z - i\omega_0 t}]$, where $k_0 = \omega_0/c$, $\mathbf{a}_0(t - z/c) = \sqrt{2I_0/\epsilon_0 c}e^{-2\ln 2(t - z/c)^2/\tau^2}\hat{\mathbf{e}}_y$ is the vectorial pulse envelope, and ϵ_0 is the dielectric permittivity of vacuum. The pump field is assumed to propagate over the z-direction and to be linearly polarized over the y-direction, indicated by the $\hat{\mathbf{e}}_y$ unit vector. Because the magnetic force produces significant effects only in the relativistic regime, it can be neglected in the weak EM excitation limit. In the linear regime, the electron mean velocity $\mathbf{v}(\mathbf{r}, t) \simeq \mathbf{v}_l(\mathbf{r}, t)$ remains unaffected by heating and satisfies the Drude model $\partial_t \mathbf{v}_l = -\gamma \mathbf{v}_l - (e/m)\mathbf{E}_{\text{in}}(\mathbf{r}, t)$, where $\mathbf{E}_{\text{in}}(\mathbf{r}, t) = \text{Re}[\mathbf{A}_{\text{in}}(\mathbf{r}, t)e^{-i\omega_0 t}]$ is the electric field within the NS, produced by the superposition of the impinging and induced pump fields. Owing to the quasi-monochromatic regime $\tau \gg 2\pi/\omega_0$, we adopt the slowly-varying envelope approximation (SVEA), where the pump vectorial envelope $\mathbf{A}_{\text{in}}(\mathbf{r}, t)$ is
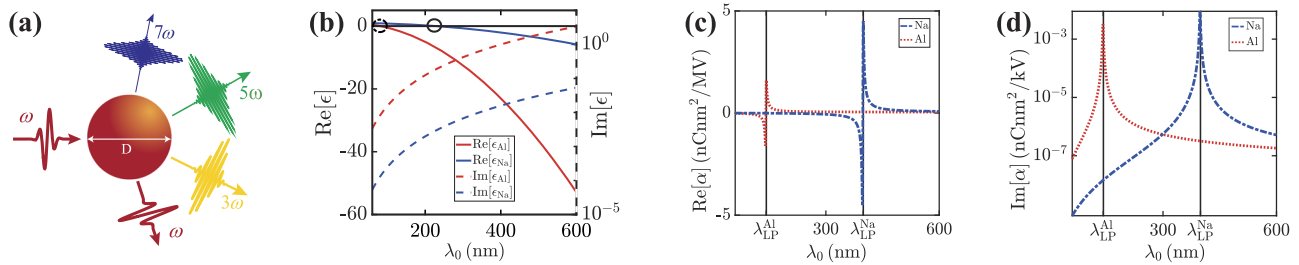
FIG. 1. (a) Schematic of the considered NSs with diameter D, illuminated by an ultrafast pump pulse with $\simeq$ps time duration and carrier angular frequency ω_0 producing harmonic generation. (b) Dependence of the RLDPs $\epsilon_{Na,Al}(\lambda_0)$ real (solid curve) and imaginary (dashed curve) parts over the pump carrier wavelength λ_0. The circles indicate the UV plasma wavelengths of Na (solid circle) and Al (dashed circle). (c) and (d) Dependence of the (c) real and (d) imaginary parts of the linear polarizabilities $\alpha_{Na,Al}$ over λ_0 for Na/Al-based NSs with $D = 15$ nm. In both plots, the solid vertical black lines indicate the LP resonance wavelengths of Na (λ_{LP}^{Na}) and Al (λ_{LP}^{Al}).

temporally modulated over a duration much longer than the single-cycle period $2\pi/\omega_0$. In turn, in such assumptions, one gets the solution $\mathbf{J}_1(\mathbf{r},t) = \epsilon_0 \, \text{Re}\{-i\omega_0[\epsilon(\omega_0) - 1]\mathbf{A}_{in}(\mathbf{r})e^{-i\omega_0 t}\}$, where $\epsilon(\omega_0) = 1 - \omega_P^2/\omega_0(\omega_0 + i\gamma)$ is the Drude relative linear dielectric permittivity (RLDP) of Na (ϵ_{Na}) or Al (ϵ_{Al}), and $\omega_P = \sqrt{n_0 e^2/\epsilon_0 m}$ is their plasma frequency. In Fig. 1(b), we illustrate the dependence of $\epsilon_{Na,Al}(\lambda_0)$ over the carrier vacuum wavelength λ_0, where the plasma frequencies ω_P ($\omega_P^{Na} \simeq 8.2 \times 10^{15}$ rad/s, $\omega_P^{Al} \simeq 2.3 \times 10^{16}$ rad/s) and the damping rates γ ($\gamma_{Na} \simeq 24.6$ ps^{-1}, $\gamma_{Al} \simeq 195.3$ ps^{-1}) of Na[36] and Al[37] are obtained from previously reported results. In the quasi-static limit where $D \ll \lambda_0$, the delay associated with radiation propagation is negligible, the induced polarization charges follow adiabatically the external field over time, and the field distribution is practically uniform within the NS. In turn, the linear polarizability of the Na-(α_{Na}) and Al-based (α_{Al}) NS can be calculated in the electrostatic approximation, yielding $\alpha(\omega_0) = \pi\epsilon_0 D^3 [\epsilon(\omega_0) - 1]/[2\epsilon(\omega_0) + 4]$ and the uniform internal field $\mathbf{A}_{in}(t) = 3/[\epsilon(\omega_0) + 2]\mathbf{a}_0(t)$.

In Figs. 1(c) and 1(d), we illustrate the dependence of the (c) real and (d) imaginary parts of the linear polarizabilities $\alpha(\lambda_0) = \alpha_{Na,Al}(\lambda_0)$ of Na and Al over the carrier vacuum wavelength λ_0. Note that at two characteristic wavelengths, the linear polarizabilities of Na (at $\lambda_{LP}^{Na} \simeq 399$ nm) and Al (at $\lambda_{LP}^{Al} \simeq 142$ nm) become resonant due to LP resonance. Conversely to noble metals where LP resonances are spectrally broad, we observe that the bandwidth of LP resonances of Al/Na-based NSs is spectrally narrow ($\Delta\lambda_0 \simeq 1$–5 nm) due to the reduced absorption accounted for by the small damping rates $\gamma_{Na,Al}$. In turn, the linear absorption cross-section of the Na/Al-based NS can be calculated through the optical theorem, yielding the quasi-static approximation $\sigma_{abs}^{Na,Al} = (k_0/\epsilon_0)\text{Im}[\alpha(\omega_0)]$. When the NS diameter becomes comparable with the driving wavelength, the quasi-static approximation does not provide accurate results, and the absorption cross-section should be calculated through the full Mie theory[38] (σ_{abs}^{Mie}). In Figs. 2(a) and 2(b), we illustrate the deviation between Mie theory and quasi-static results $|\sigma_{abs}^{Mie} - \sigma_{Na,Al}|/\sigma_{max}^{Na,Al}$ as a function of D and λ_0 for (a) Na- and (b) Al-based NSs, where $\sigma_{max}^{Na,Al} = \max[\sigma_{abs}^{Na,Al}]$ and Mie results are obtained from open-source data.[39] Note that for NS diameters $D < 20$ nm, the quasi-static approximation becomes accurate, and the approach developed below is justified. Owing to LP excitation, the induced
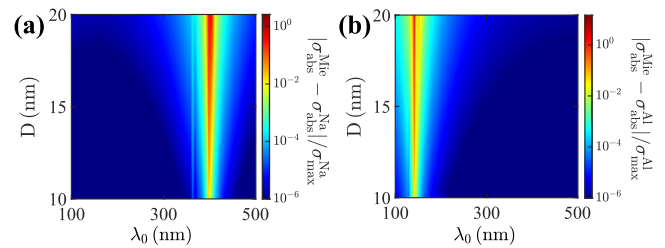

FIG. 2. (a) and (b) Color density plot illustrating the dependence of $|\sigma_{abs}^{Mie} - \sigma_{abs}^{Na,Al}|/\sigma_{Na,Al}^{max}$ over D and λ_0 for (a) Na- and (b) Al-based NSs, respectively. Such a quantity accounts for the deviation of absorption scattering cross-section calculations obtained by the full Mie theory (σ_{abs}^{Mie}) and the electrostatic approximation ($\sigma_{Na,Al}$), normalized to the maximum absorption cross section ($\sigma_{max}^{Na,Al} = \max[\sigma_{abs}^{Na,Al}]$).

surface charge density resonates, enhancing the local field intensity within the NS by a factor $F_{enh} = |A_{in}(t)/a_0(t)|^2 = 9/|\epsilon(\omega_0) + 2|^2 \simeq 10^3$–$10^5$ [$F_{enh}(\lambda_{LP}^{Na}) \simeq 3.7 \times 10^4$ for Na and $F_{enh}(\lambda_{LP}^{Al}) \simeq 4.6 \times 10^3$ for Al]. Again, we emphasize that such large field intensity enhancements arise from the reduced absorption of Na and Al in the considered spectral range. Owing to the amplified electric field produced by the considered Na/Al-based NSs, odd-order NL effects are boosted.

III. PLASMON-ENHANCED THG

In order to attain the THG NL susceptibilities of Na and Al, we follow a previously reported multiple scale expansion of Eq. (2) in the SVEA and in the weak EM excitation limit,[35] providing the THG NL polarization field $\mathbf{P}_{THG}(t) = \epsilon_0 \, \text{Re}[\chi_{coll}^{(3\omega_0)} A_{in}^2 \mathbf{A}_{in} e^{-3i\omega_0 t}]$, where $\chi_{coll}^{(3\omega_0)}(\omega_0) = (m\omega_P^2/3ie\omega_0)s_3^{(3\omega_0)}(\omega_0)$ is the collision-induced THG-NL susceptibility and

$$s_3^{(3\omega_0)} = \frac{-e^3(2\gamma - \gamma_{th})(5\gamma - \gamma_{th} - 3i\omega_0)}{40m^2 k_b T_0(\gamma_{th} - 2i\omega_0)(\gamma - 3i\omega_0)(\gamma - i\omega_0)^3}. \quad (4)$$

In our calculations, we take $m = m_{Na} \simeq 1.184 \times 10^{-30}$ kg for Na[40] and $m = m_{Al} \simeq 1.275 \times 10^{-30}$ kg for Al.[40] To the best of our knowledge, quantitative measurements of the thermalization rate of conduction
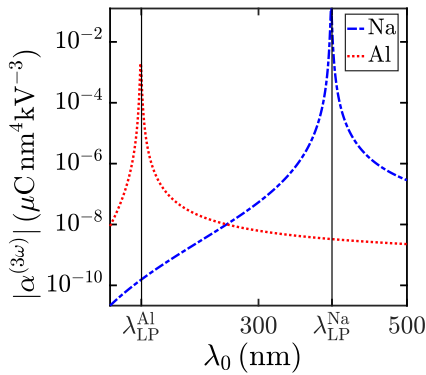
FIG. 3. Dependence of the THG polarizability modulus $|\alpha^{(3\omega_0)}|$ over λ_0 for Na- (blue dot-dashed line) and Al-based (red dotted line) NSs with fixed diameter $D = 15$ nm. The black solid vertical lines indicate λ_{LP}^{Na} and λ_{LP}^{Al}.

electrons in Na are lacking, and thus we assume that they relax to equilibrium over the same timescale of gold[41] $\gamma_{th} = \gamma_{th}^{Na} = (300 \text{ fs})^{-1}$. Conversely, the hot conduction electron relaxation rate in Al $\gamma_{th} = \gamma_{th}^{Al} = (500 \text{ fs})^{-1}$ has been measured by transient extinction spectroscopy.[42] We emphasize that the obtained expressions for the THG-NL susceptibilities of Na and Al account for *collision-driven nonlinearity*. In principle, in such materials also, band anharmonicity and off-resonant interband transitions could provide contributions to the NL response. However, as the scope of our work lies in the modeling of collision-driven nonlinear radiation–matter interaction, we do not account for such contributions in our calculations. The THG-NL polarization generates a pulsed electric dipole moment oscillating at carrier frequency $3\omega_0$, explicitly given by

$$\mathbf{d}_{THG}(t) = \int_{\tau_{sph}} \mathbf{P}_{THG}(t) d\tau_{sph}$$
$$= \text{Re}\left[\alpha^{(3\omega_0)}(\omega_0) a_0^2(t) \mathbf{a}_0(t) e^{-3i\omega_0 t}\right], \quad (5)$$

where $\alpha^{(3\omega_0)}(\omega_0) = \tau_{sph}\epsilon_0 \chi_{coll}^{(3\omega_0)} \{3/[\epsilon(\omega_0) + 2]\}^3$ is the THG NL polarizability and $\tau_{sph} = (4/3)\pi R^3$. In Fig. 3, we depict the dependence of $|\alpha^{(3\omega_0)}(\lambda_0)|$ over the pump carrier wavelength λ_0 for Na

(dot-dashed blue line) and Al (dotted red line) based NSs with diameter $D = 15$ nm. Note that, owing to the field enhancement produced by the NSs, the THG-NL polarizabilities are boosted at the LP resonance by a factor $\simeq 10^6$ for Na (at λ_{LP}^{Na}) and by a factor $\simeq 10^5$ for Al (at λ_{LP}^{Al}). Hence, the electric $\mathbf{E}_{dip}^{THG}(\mathbf{r}, t)$ and magnetic $\mathbf{H}_{dip}^{THG}(\mathbf{r}, t)$ fields produced by the NL oscillating dipoles of the NSs in the far field can be readily calculated by the Green function approach, providing an analytical expression for the time-dependent Poynting vector of the emitted THG pulses $\mathbf{S}_{THG}(\mathbf{r}, t) = \langle \mathbf{E}_{dip}^{THG}(\mathbf{r}, t) \times \mathbf{H}_{dip}^{THG}(\mathbf{r}, t)\rangle_T$, where $\langle \cdots \rangle_T$ indicates the time average over the single-cycle duration $T = 2\pi/\omega_0$. In the far field region $\mathbf{S}_{THG}(\mathbf{r}, t) \propto \hat{\mathbf{e}}_r/r^2$ and in turn the THG emitted power at distance r is pulsed $P_{THG}(r, t) = \int_0^{2\pi} d\phi \int_0^\pi d\theta r^2 \sin\theta \mathbf{S}_{THG}(\mathbf{r}, t) \cdot \hat{\mathbf{e}}_r = P_{THG}^{peak} e^{-12 \ln 2(t-r/c)^2/\tau^2}$, where $P_{THG}^{peak} = 54\omega_0^4|\alpha^{(3\omega_0)}(\omega_0)|^2 I_0^3/\pi\epsilon_0^4 c^6$, the position distance affects only the time delay and the peak power P_{THG}^{peak} does not depend over r.

In Figs. 4(a)–4(d), we illustrate the dependence of the THG radiated peak power P_{THG}^{peak} by (a) and (c) Na- and (b) and (d) Al-based NSs over (a) and (b) the pump carrier wavelength λ_0 and (c) and (d) its peak intensity I_0. Note that, owing to the peaked THG-NL polarizability at the Na/Al LP resonances $\lambda_{LP}^{Na,Al}$, the THG radiated power is enhanced by a factor $\simeq 10^{12}$ (in Na-based NSs) and $\simeq 10^{10}$ (in Al-based NSs). We also emphasize that in Al-based NSs, the THG process is reduced with respect to Na-based NSs owing to their inherently weaker collision-driven THG-NL susceptibility $|\chi_{coll,Al}^{3\omega_0}(\lambda_{LP}^{Al})| \simeq 10^{-1}|\chi_{coll,Na}^{3\omega_0}(\lambda_{LP}^{Na})|$.[35] Moreover, due to the perturbative nature of the considered THG-NL process, the emitted THG peak power $P_{THG}^{peak} \propto I_0^3$ depends cubically over the pump peak intensity reaching orders of $\simeq 10^{-4}$ W in Na-based NSs and $\simeq 10^{-7}$ W in Al-based NSs for $I_0 = 1$ GW/cm^2, see Figs. 4(c) and 4(d). Even though the THG process in Al-based NSs is weaker, it is worth highlighting that it produces photon energies >20 eV in the XUV spectral range due to the smaller LP resonance wavelength $\lambda_{LP}^{Al} = 142$ nm $<\lambda_{LP}^{Na} = 399$ nm. In addition, the THG process produces pulse compression by a factor $1/\sqrt{3}$ and the dipolar emission occurs uniformly over the whole azimuthal angle while being peaked at the equatorial circle denoted by the $\pi/2$ zenithal angle. In this respect, we envisage that collective resonances in Na/Al-based NS arrays may provide a viable platform for directional THG emission.[43]
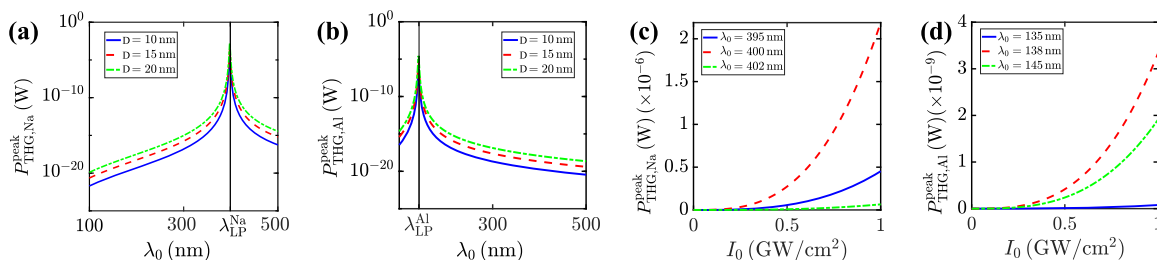

FIG. 4. Dependence of the THG emitted peak power $P_{THG}^{peak}(\lambda_0, I_0)$ by (a) and (c) Na- and (b) and (d) Al-based NSs over (a) and (b) λ_0 and (c) and (d) I_0. (a) and (b) Plots are obtained for several distinct NS diameters $D = 10, 15, 20$ nm and fixed $I_0 = 1$ GW/cm^2. The black vertical lines indicate the LP resonance wavelengths $\lambda_{LP}^{Na,Al}$. (c) and (d) Plots are obtained for fixed $D = 15$ nm and several distinct (c) $\lambda_0 = 395, 400, 402$ nm and (d) $\lambda_0 = 135, 138, 145$ nm.
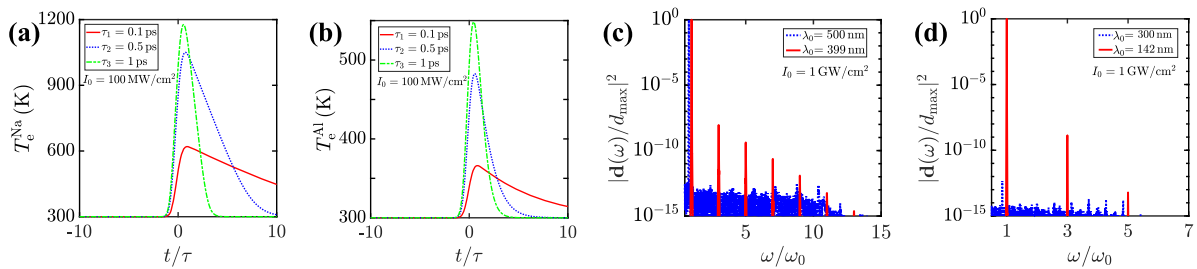
FIG. 5. (a) and (b) Temporal evolution of the electronic temperature T_e for fixed pump peak intensity $I_0 = 100$ MW/cm^2 and several diverse pulse durations $\tau = 0.1, 0.5, 1$ ps for (a) $\lambda_0 = \lambda_{LP}^{Na} = 399$ nm in Na-based NSs, and (b) $\lambda_0 = \lambda_{LP}^{Al} = 142$ nm in Al-based NSs, both with diameter $D = 15$ nm. (c) and (d) Dependence of the dipole moment power spectrum $|\mathbf{d}(\omega)|^2$ [rescaled to its maximum $|d_{max}|^2 = \max_\omega |\mathbf{d}(\omega)|^2$] over ω/ω_0 for fixed $D = 15$ nm and $I_0 = 1$ GW/cm^2, and (c) Na- and (d) Al-based NSs upon diverse pump carrier wavelengths (c) $\lambda_0 = 399, 500$ nm and (d) $\lambda_0 = 142, 300$ nm.

IV. PLASMON-ENHANCED HHG

The considered collision-driven harmonic-generation process ensues from the fast temporal oscillations of the nonlinearly-saturated instantaneous absorbed power density, accounted by $\mathcal{F}_\gamma$ and Q in Eq. (2). Such a saturated absorption arises from the quenching of el–el and el–ph grazing collisions upon strong-field excitation due to their reduced interaction time with the scattering center.[34] Such fast oscillations are the ones responsible for THG described in the Sec. III and lead to HHG for intense EM excitation. Modeling of higher order harmonic generation requires the non-perturbative solution of Eq. (2), which we undertake numerically in the undepleted-pump approximation by a fourth-order Runge-Kutta algorithm by considering the electric force acting on the NS conduction electrons $\mathbf{F}_{eff} = -e\mathbf{E}_{in}(\mathbf{r}, t)$. In Figs. 5(a) and 5(b), we illustrate the temporal evolution of the out-of-equilibrium electron temperature T_e for several distinct pump pulse durations and fixed peak intensity $I_0 = 100$ Mw/cm^2 for (a) Na- and (b) Al-based NSs at their LP resonant wavelengths $\lambda_{LP}^{Na,Al}$. Note that the electronic temperature increase in Al-based NSs is smaller owing to the reduced field enhancement with respect to Na-based NSs. The obtained numerical results for the instantaneous mean electron velocity $\mathbf{v}(t)$ enable the calculation of the instantaneous dipole moment spectrum in the SVEA by a fast Fourier transform algorithm providing

$\mathbf{d}(\omega) = (-ien_0\tau_{sph}/\omega)\mathbf{v}(\omega)$. In Figs. 5(c) and 5(d), we depict the calculated electric dipole power spectrum $|\mathbf{d}(\omega)/d_{max}|^2$, where $|d_{max}|^2 = \max_\omega |\mathbf{d}(\omega)|^2$ for (c) Na- and (d) Al-based NSs with diameter $D = 15$ nm pumped at their LP resonant wavelengths with pump peak intensity $I_0 = 1$ GW/cm^2. We observe that the considered NSs produce HHG (c) up to the 13th (in Na-based NSs) and (d) fifth harmonic (in Al-based NSs) with conversion efficiency $>10^{-15}$ in the XUV spectral range. To fairly assess the plasmon-induced HHG process, in Fig. 6, we illustrate the dependence of $|\mathbf{d}(\omega)/d_{max}|^2$ over ω and the pump wavelength λ_0 for (a) Na- and (b) Al-based NSs at the same pump peak intensity $I_0 = 1$ GW/cm^2. Note that in both cases, the maximum efficiency is attained near the LP wavelength $\lambda_{LP}^{Na/Al}$ (slightly shifted due to Ohmic losses), see the black dashed lines in Figs. 6(a) and 6(b). We also emphasize that our calculations are based on the electric dipole approximation, which breaks for sufficiently higher harmonics in the highly non-perturbative regime where the field intensity of the higher harmonics becomes comparable with the pump field intensity. However, due to the weak radiation–matter interaction in the considered spectral range, such a regime is not attainable and the undepleted pump approximation is valid. Indeed, the HHG weights of the dipolar power spectrum are much smaller than one, see Figs. 5 and 6. In turn, in the undepleted pump approximation and in the pump quasi-static regime the field radiated by the nanosphere is purely dipolar.

We also highlight that both perturbative and non-perturbative calculations predict only odd-order harmonic generation. Such observations arise from (i) the neglection of nonlocal contributions to collision-driven nonlinearity accounted by the GHM in Eq. (2) and (ii) the centrosymmetric geometry of the considered NSs. In principle, similarly to intraband anharmonicity and interband dynamics, also collision-driven nonlinearity can produce even-order harmonics by the nonlocal convective nonlinearity of the GHM,[34,35] neglected in this paper. In turn, we anticipate that HHG in nanoparticles with more complex geometric features is expected to display shape-dependent spectra arising from non-destructive interference of surface nonlinear contributions to the HHG process.[44,45] Moreover, surface roughness, nonlocality, finite-size effects, and electronic spill-out may provide resonance shifts and absorption corrections,[46] becoming dominant for $D < 10$ nm. The accounting of such corrections requires more advanced numerical tools, for example, quantum hydrodynamic frequency domain calculations.[47,48]
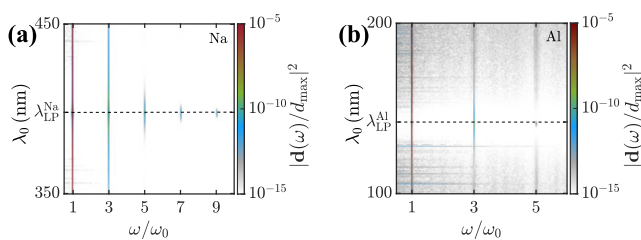

FIG. 6. Color density plot illustrating the dependence of the electric dipole power spectrum $|\mathbf{d}(\omega)/d_{max}|$ over the pump wavelengths λ_0 and ω/ω_0 for Na (a) and Al (b), respectively. The dashed black lines represent the LP resonance wavelengths $\lambda_{LP}^{Na/Al}$. All plots are obtained for a fixed pump peak intensity of $I_0 = 1$ GW/cm^2.

18 December 2024 14:12:57

V. CONCLUSIONS

In conclusion, we explored the potential of poor metal-based nanostructures for plasmon-enhanced harmonic generation. By focusing on Na/Al-based NSs, we have modeled the harmonic generation process by a GHM accounting non-perturbatively for el–el and el–ph grazing collisions. By perturbatively solving the GHM equations upon ultrafast EM pumping, we have derived analytical expressions for the THG-NL polarizabilities of Na/Al-based NSs. Our results indicate that LP resonances in such nanostructures enable the efficient enhancement of the local field by 10^3–10^5, leading to plasmon-enhanced THG. Furthermore, by numerically solving the GHM equations, we found that Na/Al-based NSs produce HHG up to (Na) 15th harmonic and (Al) fifth harmonic with conversion efficiencies $>10^{-15}$ in the XUV spectral range. Our results shed light on the possibilities offered by poor metals for advanced nanosources of XUV radiation that may find application in future nano-spectroscopy devices.

AUTHOR DECLARATIONS

Conflict of Interest

The authors have no conflicts to disclose.

Author Contributions

Matteo Silvestri: Data curation (equal); Formal analysis (equal); Investigation (equal); Methodology (equal); Software (equal); Visualization (equal); Writing – original draft (equal); Writing – review & editing (equal). **Matteo Venturi**: Data curation (equal); Formal analysis (equal); Investigation (equal); Methodology (supporting); Software (supporting); Visualization (equal); Writing – original draft (supporting); Writing – review & editing (equal). **Mattia Di Muzio**: Data curation (equal); Formal analysis (equal); Investigation (equal); Methodology (supporting); Software (supporting); Visualization (equal); Writing – original draft (supporting); Writing – review & editing (equal). **Raju Adhikary**: Data curation (supporting); Formal analysis (supporting); Investigation (supporting); Methodology (supporting); Software (supporting); Visualization (supporting); Writing – original draft (supporting); Writing – review & editing (equal). **Carino Ferrante**: Investigation (supporting); Methodology (supporting); Project administration (supporting); Supervision (supporting); Visualization (supporting); Writing – original draft (supporting); Writing – review & editing (equal). **Paola Benassi**: Formal analysis (supporting); Investigation (supporting); Methodology (supporting); Supervision (supporting); Writing – original draft (supporting); Writing – review & editing (equal). **Andrea Marini**: Conceptualization (equal); Formal analysis (equal); Funding acquisition (equal); Investigation (equal); Methodology (equal); Project administration (equal); Software (equal); Supervision (equal); Visualization (equal); Writing – original draft (equal); Writing – review & editing (equal).

DATA AVAILABILITY

The data that support the findings of this study are available within the article.

REFERENCES

[1] M. Kauranen and A. V. Zayats, "Nonlinear plasmonics," Nat. Photonics **6**, 737–748 (2012).

[2] K. Wang et al., "Plasmon-enhanced optical nonlinearity for femtosecond all-optical switching," Appl. Phys. Lett. **111**, 181102 (2017).

[3] A. Marini and F. Biancalana, "Ultrashort self-induced transparency plasmon solitons," Phys. Rev. Lett. **110**, 243901 (2013).

[4] M. Lippitz, M. A. van Dijk, and M. Orrit, "Third-harmonic generation from single gold nanoparticles," Nano Lett. **5**, 799–802 (2005).

[5] P. Ginzburg et al., "Nonperturbative hydrodynamic model for multiple harmonics generation in metallic nanostructures," ACS Photonics **2**, 8–13 (2015).

[6] I. A. Calafell et al., "Giant enhancement of third-harmonic generation in graphene–metal heterostructures," Nat. Nanotechnol. **16**, 318–324 (2021).

[7] D. V. Skryabin, A. V. Gorbach, and A. Marini, "Surface-induced nonlinearity enhancement of TM modes in planar subwavelength waveguides," J. Opt. Soc. Am. B **28**, 109–114 (2011).

[8] A. Marini et al., "Surface-induced nonlinearity enhancement in subwavelength rod waveguides," Phys. Rev. A **84**, 063839 (2011).

[9] I. Abdulhalim, "Coupling configurations between extended surface electromagnetic waves and localized surface plasmons for ultrahigh field enhancement," Nanophotonics **7**, 1891–1916 (2018).

[10] A. Fafin et al., "Surface plasmon resonances and local field enhancement in aluminum nanoparticles embedded in silicon nitride," J. Phys. Chem. C **123**, 13908–13917 (2019).

[11] Y. Wu et al., "Intrinsic optical properties and enhanced plasmonic response of epitaxial silver," Adv. Mater. **26**, 6106–6110 (2014).

[12] M. A. Noginov et al., "Stimulated emission of surface plasmon polaritons," Phys. Rev. Lett. **101**, 226806 (2008).

[13] A. Marini et al., "Amplification of surface plasmon polaritons in the presence of nonlinearity and spectral signatures of threshold crossover," Opt. Lett. **34**, 2864–2866 (2009).

[14] P. M. Bolger et al., "Amplified spontaneous emission of surface plasmon polaritons and limitations on the increase of their propagation length," Opt. Lett. **35**, 1197–1199 (2010).

[15] P. Berini and I. De Leon, "Surface plasmon-polariton amplifiers and lasers," Nat. Photonics **6**, 16–24 (2012).

[16] F. Bonaccorso et al., "Graphene photonics and optoelectronics," Nat. Photonics **4**, 611–622 (2010).

[17] F. J. García de Abajo, "Graphene plasmonics: Challenges and opportunities," ACS Photonics **1**, 135–152 (2014).

[18] G. V. Naik, J. Kim, and A. Boltasseva, "Oxides and nitrides as alternative plasmonic materials in the optical range (invited)," Opt. Mater. Express **1**, 1090–1099 (2011).

18 December 2024 14:12:57

[19] J. Kim *et al.*, "Optical properties of gallium-doped zinc oxide—A low-loss plasmonic material: First-principles theory and experiment," Phys. Rev. X **3**, 041037 (2013).

[20] G. V. Naik, V. M. Shalaev, and A. Boltasseva, "Alternative plasmonic materials: Beyond gold and silver," Adv. Mater. **25**, 3264–3294 (2013).

[21] N. Kinsey, C. DeVault, A. Boltasseva, and V. M. Shalaev, "Near-zero-index materials for photonics," Nat. Rev. Mater. **4**, 742–760 (2019).

[22] M. Z. Alam, I. De Leon, and R. W. Boyd, "Large optical nonlinearity of indium tin oxide in its epsilon-near-zero region," Science **352**, 795–797 (2016).

[23] I. Liberal and N. Engheta, "Near-zero refractive index photonics," Nat. Photonics **11**, 149–158 (2017).

[24] D. Powell *et al.*, "Nonlinear control of tunneling through an epsilon-near-zero channel," Phys. Rev. B **79**, 245135 (2009).

[25] M. A. Vincenti, D. de Ceglia, A. Ciattoni, and M. Scalora, "Singularity-driven second- and third-harmonic generation at ϵ-near-zero crossing points," Phys. Rev. A **84**, 063826 (2011).

[26] T. S. Luk *et al.*, "Enhanced third harmonic generation from the epsilon-near-zero modes of ultrathin films," Appl. Phys. Lett. **106**, 151103 (2015).

[27] A. Marini and F. J. García de Abajo, "Self-organization of frozen light in near-zero-index media with cubic nonlinearity," Sci. Rep. **6**, 20088 (2016).

[28] Y. Yang *et al.*, "High-harmonic generation from an epsilon-near-zero material," Nat. Phys. **15**, 1022–1026 (2019).

[29] M. Semmlinger *et al.*, "Generating third harmonic vacuum ultraviolet light with a TiO_2 metasurface," Nano Lett. **19**, 8972–8978 (2019).

[30] A. Ahmadivand and B. Gerislioglu, "Deep- and vacuum-ultraviolet metaphotonic light sources," Mater. Today **51**, 208–221 (2021).

[31] S. Nie and Y. Guan, "Review of UV laser and its applications in micromachining," Opto-Electron. Eng. **44**, 1169 (2017).

[32] M. Lewenstein, P. Balcou, M. Y. Ivanov, A. L'Huillier, and P. B. Corkum, "Theory of high-harmonic generation by low-frequency laser fields," Phys. Rev. A **49**, 2117 (1994).

[33] L. Assogna, C. Ferrante, A. Ciattoni, and A. Marini, "XUV plasmonic waveguides by near-zero index heterostructures," J. Phys. Photonics **5**, 045001 (2023).

[34] A. Marini, A. Ciattoni, and C. Conti, "Out-of-equilibrium electron dynamics of silver driven by ultrafast electromagnetic fields—A novel hydrodynamical approach," Faraday Discuss. **214**, 235–243 (2019).

[35] M. Silvestri *et al.*, "Resonant third-harmonic generation driven by out-of-equilibrium electron dynamics in sodium-based near-zero index thin films," Nanophotonics **13**, 2003–2013 (2024).

[36] F. Forstmann and R. R. Gerhardt, *Metal Optics Near the Plasma Frequency* (Springer-Verlag, 1986).

[37] H. Ehrenreich, H. R. Philipp, and B. Segall, "Optical properties of aluminum," Phys. Rev. **132**, 1918–1928 (1963).

[38] V. Myroshnychenko, J. Rodríguez-Fernández, I. Pastoriza-Santos, A. M. Funston, C. Novo, P. Mulvaney, L. M. Liz-Marzán, and F. J. García de Abajo, "Modelling the optical response of gold nanoparticles," Chem. Soc. Rev. **37**, 1792–1805 (2008).

[39] See http://widgets.nanophotonics.es/mie/index.html for information about Mie light scattering by a single sphere database.

[40] N. Ashcroft and N. Mermin, *Solid State Physics* (Holt-Saunders, 1976).

[41] C. K. Sun, F. Vallée, L. H. Acioli, E. P. Ippen, and J. G. Fujimoto, "Femtosecond-tunable measurement of electron thermalization in gold," Phys. Rev. B **50**, 15337 (1994).

[42] M.-N. Su *et al.*, "Ultrafast electron dynamics in single aluminum nanostructures," Nano Lett. **19**, 3091–3097 (2019).

[43] F. J. García de Abajo, "Colloquium: Light scattering by particle and hole arrays," Rev. Mod. Phys. **79**, 1267–1290 (2007).

[44] M. Zavelani-Rossi, M. Celebrano, P. Biagioni, D. Polli, M. Finazzi, L. Duó, G. Cerullo, M. Labardi, M. Allegrini, J. Grand, and P.-M. Adam, "Near-field second-harmonic generation in single gold nanoparticles," Appl. Phys. Lett. **92**, 093119 (2008).

[45] A. Babaze, R. Esteban, J. Aizpurua, and A. G. Borisov, "Second-harmonic generation from a quantum emitter coupled to a metallic nanoantenna," ACS Photonics **7**, 701–713 (2020).

[46] P. A. D. Goncalves, T. Christensen, N. Rivera, A.-P. Jauho, N. A. Mortensen, and M. Soljacic, "Plasmon–emitter interactions at the nanoscale," Nat. Commun. **11**, 366 (2020).

[47] M. Khalid, F. Della Sala, and C. Ciracì, "Optical properties of plasmonic core-shell nanomatryoshkas: A quantum hydrodynamic analysis," Opt. Express **26**, 17322–17334 (2018).

[48] C. Ciracì, F. Vidal-Codina, D. Yoo, J. Peraire, S.-H. Oh, and D. R. Smith, "Impact of surface roughness in nanogap plasmonic systems," ACS Photonics **7**, 908–913 (2020).

18 December 2024 14:12:57